

# Anisotropic Mechanical Properties of ABS Parts Fabricated by Fused Deposition Modelling

Constance Ziemian<sup>1</sup>, Mala Sharma<sup>1</sup> and Sophia Ziemian<sup>2</sup>

<sup>1</sup>*Bucknell University,*

<sup>2</sup>*Duke University,*

*USA*

## 1. Introduction

Layered manufacturing (LM) methods have traditionally been used for rapid prototyping (RP) purposes, with the primary intention of fabricating models for visualization, design verification, and kinematic functionality testing of developing assemblies during the product realization process (Caulfield et al., 2007). Without any need for tooling or fixturing, LM allows for the computer-controlled fabrication of parts in a single setup directly from a computerized solid model. These characteristics have proven beneficial in regard to the objective of reducing the time needed to complete the product development cycle (Chua et al., 2005).

There are numerous LM processes available in the market today, including stereolithography (SLA), fused deposition modeling (FDM), selective laser sintering (SLS), and three-dimensional printing (3DP), all of which are additive processes sharing important commonalities (Upcraft & Fletcher, 2003). For each of these processes, the object design is first represented as a solid model within a computer aided design (CAD) software package and then exported into tessellated format as an STL file. This faceted model is then imported into the relevant LM machine software where it is mathematically sliced into a series of parallel cross-sections or layers. The software creates a machine traverse path for each slice, including instructions for the creation of any necessary scaffolding to support overhanging slice portions. The physical part is then fabricated, starting with the bottom-most layer, by incrementally building one model slice on top of the previously built layer. This additive layering process is thus capable of fabricating components with complex geometrical shapes in a single setup without the need for tooling or human intervention or monitoring.

In recent years, layered manufacturing processes have begun to progress from rapid prototyping techniques towards rapid manufacturing methods, where the objective is now to produce finished components for potential end use in a product (Caulfield et al., 2007). LM is especially promising for the fabrication of specific need, low volume products such as replacement parts for larger systems. This trend accentuates the need, however, for a thorough understanding of the associated mechanical properties and the resulting behaviour of parts produced by layered methods. Not only must the base material be durable, but the mechanical properties of the layered components must be sufficient to meet in-service loading and operational requirements, and be reasonably comparable to parts produced by more traditional manufacturing techniques.

Fused deposition modeling (FDM) by Stratasys Inc. is one such layered manufacturing technology that produces parts with complex geometries by the layering of extruded materials, such as durable acrylonitrile butadiene styrene (ABS) plastic (Figure 1). In this process, the build material is initially in the raw form of a flexible filament. The feedstock filament is then partially melted and extruded through a heated nozzle within a temperature controlled build environment. The material is extruded in a thin layer onto the previously built model layer on the build platform in the form of a prescribed two-dimensional (x-y) layer pattern (Sun et al., 2008). The deposited material cools, solidifies, and bonds with adjoining material. After an entire layer is deposited, the build platform moves downward along the z-axis by an increment equal to the filament height (layer thickness) and the next layer is deposited on top of it.

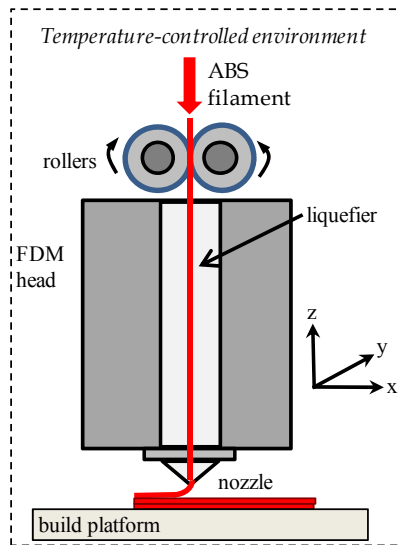


Fig. 1. Schematic of the FDM process

If the model requires structural support for any overhanging geometry, a second nozzle simultaneously extrudes layers of a water soluble support material in this same manner. Once the build process is completed, the support material is dissolved and the FDM part can be viewed as a laminate composite structure with vertically stacked layers of bonded fibers or rasters (Sood et al., 2011). Consequently, the mechanical properties of FDM parts are not solely controlled by the build material of the original filament, but are also significantly influenced by a directionally-dependent production process that fabricates components with anisotropic characteristics associated with the inherent layering.

Several researchers have specifically considered the anisotropic characteristics of FDM parts in recent years. Rodriguez et al. (2001) investigated the tensile strength and elastic modulus of FDM specimens with varying mesostructures in comparison with the properties of the ABS monofilament feedstock. They determined that the tensile strength was the greatest for parts with fibers aligned with the axis of the tension force. Ahn et al. (2002) designed a factorial experiment to quantify the effects of model temperature, bead width, raster

orientation, air gap, and ABS color on both tensile and compressive strengths of FDM parts. It was determined that both air gap and raster orientation had significant effects on the resulting tensile strength, while compressive strength was not affected by these factors. Their results include a set of recommended build rules for designing FDM parts. A similar study was completed by Sood et al. (2010), with varying factors of layer thickness, build orientation, raster angle, raster width, and air gap. These researchers implemented a central composite experiment design and analyzed the functional relationship between process parameters and specimen strength using response surface methodology. Their results indicate that the tested factors influence the mesostructural configuration of the built part as well as the bonding and distortion within the part. On the basis of this work, Sood et al. (2011) further examined the effect of the same five process parameters on the subsequent compressive strength of test specimens. Their work provides insight into the complex dependency of compressive stress on these parameters and develops a statistically validated predictive equation. Results display the importance of fiber-to-fiber bond strength and the control of distortion during the build process. Lee et al. (2005) concluded that layer thickness, raster angle, and air gap influence the elastic performance of compliant ABS prototypes manufactured by fused deposition. A study conducted by Es Said et al. (2000) analyzed the effect of raster orientation and the subsequent alignment of polymer molecules along the direction of deposition during fabrication. These researchers considered the issue of volumetric shrinkage and raster orientation with respect to tensile, flexural and impact strengths. Lee et al. (2007) focused on the compressive strength of layered parts as a function of build direction. They determined that the compressive strength is greater for the axial FDM specimens than for the transverse. The foregoing studies reveal the directional dependence or anisotropy of the mechanical properties of FDM parts as a result of mesostructure and fiber-to-fiber bond strength, and provide numerous insights and recommendations regarding significant process parameters and the development of component build rules.

The goal of this project is to quantitatively analyze the potential of fused deposition modeling to fully evolve into a rapid manufacturing tool. The project objective is to develop an understanding of the dependence of the mechanical properties of FDM parts on raster orientation and to assess whether these parts are capable of maintaining their integrity while under service loading. The study utilizes the insights provided by previous researchers and further examines the effect of fiber orientation on a variety of important mechanical properties of ABS components fabricated by fused deposition modeling. This study uses FDM build recommendations provided in previous work, as well as the defined machine default values, in order to focus analysis specifically on the significant issue of fiber or raster orientation, i.e. the direction of the polymer beads (roads) relative to the loading direction of the part. Tensile, compressive, flexural, impact, and fatigue strength properties of FDM specimens are examined, evaluated, and placed in context in comparison with the properties of injection molded ABS parts.

## **2. Experimental procedure**

### **2.1 Materials**

All of the FDM specimens tested and analyzed in this study were acrylonitrile butadiene styrene (ABS). ABS is a carbon chain copolymer belonging to styrene ter-polymer chemical

family. It is a common thermoplastic that is formed by dissolving butadiene-styrene copolymer in a mixture of acrylonitrile and styrene monomers, and then polymerizing the monomers with free radical initiators (O'dian, 2004). The result is a long chain of polybutadiene crisscrossed with shorter chains of poly(styrene-co-acrylonitrile). The advantage of ABS is that it combines the strength and rigidity of the acrylonitrile and styrene polymers with the toughness of the polybutadiene rubber. The proportions can vary from 15 to 35% acrylonitrile, 5 to 30% butadiene, and 40 to 60% styrene. In this study, the resulting composition was 90-100% acrylonitrile/butadiene/styrene resin, with 0-2% mineral oil, 0-2% tallow, and 0-2% wax.

## 2.2 Specimen preparation and equipment

This project included five different mechanical tests: tension, compression, flexural (3-point bend), impact, and tension-tension fatigue. Three unique specimen designs were required. The tension, flexural, and fatigue specimens were all thin rectangular slabs (Figure 2a) fabricated to be 190.5 mm long, 12.7 mm wide, and 2.6 mm thick in accordance with ASTM D3039 (ASTM, 1998), ASTM D790 (ASTM, 2007), and ASTM D3479 (ASTM, 2007a) standards respectively. Compression specimens were cylindrical and fabricated with dimensions conforming to the ASTM D695 standard (ASTM, 1996). Each cylinder was 25.4 mm long and 12.7 mm diameter (Figure 2b). Impact specimens were fabricated with dimensions conforming to the ASTM D256 standard (ASTM, 2010). The geometry was a v-notched rectangular block of 63.5 mm long, 25.4 mm wide, and 25.4 mm thick (Figure 2c). The v-notch was modeled within the computer solid model of the specimen and was produced directly on the FDM machine.

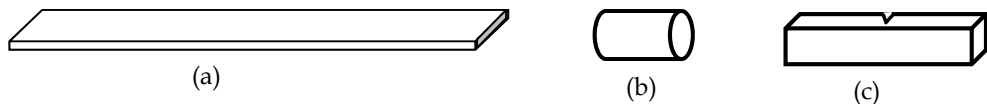


Fig. 2. Specimen geometries associated with each test

All FDM specimens were fabricated with a Stratasys Vantage-*i* machine. Solid models were first created using Pro/Engineer® software, and then tessellated and exported in STL format. Digital models were then sliced using the Vantage machine's Insight software, and layer extrusion tool paths were generated, i.e. raster patterns used to fill interior regions of each layer, to represent the four different fiber orientations studied in each test.

Layered specimens were all fabricated in a build orientation that aligned the minimum part dimension with the z-axis of the machine, i.e. perpendicular to the build platform. In this orientation, five to ten replicate specimens were built with each of four different raster patterns relative to the part loading direction, for each of the five different tests completed. The four raster orientations included: (a) longitudinal or  $0^\circ$ , i.e. rasters aligned with long dimension of the specimen, (b) diagonal or  $45^\circ$ , i.e. rasters at  $45^\circ$  to the long dimension of the specimen, (c) transverse or  $90^\circ$ , i.e. rasters perpendicular to long dimension of the specimen, and (d) default or  $+45^\circ/-45^\circ$  criss-cross, i.e. representing the machine's default raster orientation (Figure 3).

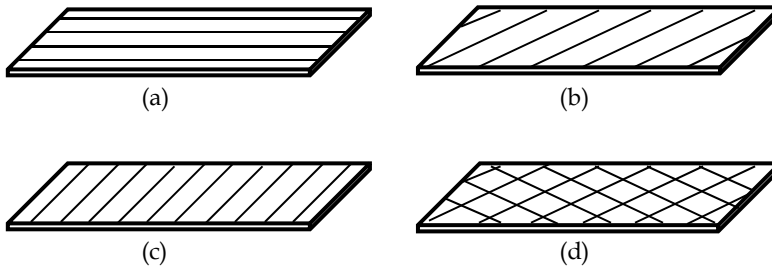


Fig. 3. Four different raster orientations investigated

All FDM specimens were built while holding all other machine process settings at the recommended or default values displayed in Table 1.

Factor	Value/Level
Air gap	0.0 mm
Nozzle	T12
Road width	0.3048 mm
Slice height	0.1778 mm
Part interior fill style	Solid normal
Part fill style	Perimeter/raster
Liquefier temperature	320 °C
Envelope temperature	80 °C

Table 1. Fixed FDM process settings

In order to measure the reference strength and behaviour of the ABS filament material, for comparisons with the layered parts, additional specimens were fabricated by injection molding for the same five tests. Aluminium molds for each of the three previously described geometries (Figure 2) were designed using Pro/Engineer® software, and manufactured on a Haas VF-1 CNC machining center. Mold cavity dimensions were the same as those described for the FDM specimens, with slight increases to compensate for the shrinkage of molded ABS at approximately 0.005 cm/cm. Parting lines and runners were located with an effort to avoid potential stress concentrations or anomalies in the resulting specimens that might affect test results. All molded specimens were fabricated from the same material as the layered models by feeding the FDM-ABS filament into a polymer granulator and cutting it into pellets of 3-5 mm in length. The pellets were then fed into the hopper of a Morgan Press G-100T injection molding machine. Molding parameters were set to the recommended values for ABS plastic, including nozzle temperature of 270 °C, mold preheat temperature of 120° C, clamping force of 71 kN (16,000 lb), and injection pressure of 41 MPa (6000 psi). Ten replicate specimens were molded for each of the five tests.

Tensile, compressive, flexural, and tension-fatigue tests were performed on an Instron model 3366 dual column uniaxial material testing with .057 micron displacement precision and up to 0.001 N force accuracy. The machine has a 10kN load force capacity. Impact strength was studied on a TMI impact tester. Resulting fracture surfaces were subsequently prepared by gold sputtering and analyzed with a JSM 500-type JEOL Scanning Electron Microscope (SEM).

### 3. Results and discussion

#### 3.1 Tension testing

The tension specimens were thin rectangular slabs made in compliance with ASTM D3039 (ASTM, 1998). Fabrication utilized the FDM T12-nozzle, providing an individual layer or slice height of 0.1778 mm. The specimen thickness of 2.6 mm was subsequently achieved with a total of 15 layers (Figure 4).

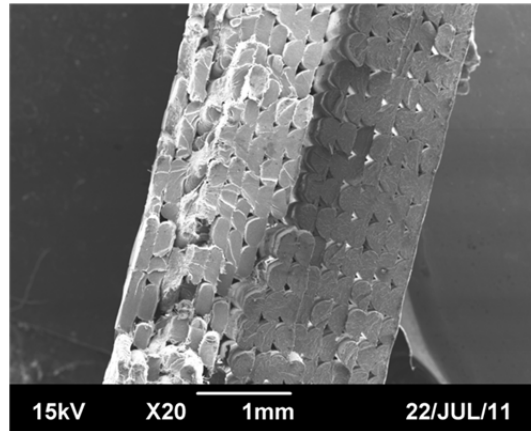


Fig. 4. SEM image displaying 15 layer thickness

A summary of the tension test results for the four raster orientations is displayed in Table 2. The mean ultimate and yield strengths (0.2% offset) were largest for the longitudinal ( $0^\circ$ ) raster orientation, 25.72 and 25.51 MPa respectively, and weakest for the transverse ( $90^\circ$ ) raster orientation, 14.56 and 14.35 MPa respectively. The mean ultimate strength of the  $90^\circ$  specimens represented only 56.23% of that of the  $0^\circ$  raster specimens, followed by the  $45^\circ$  specimens at 61.45% and the  $+45^\circ/-45^\circ$  specimens at 74.09%.

<i>Raster Orientation</i>	<i>Mean Yield Strength (MPa), Std Dev</i>	<i>Mean Ultimate Strength (MPa), Std Dev</i>	<i>Mean Effective Modulus (MPa), Std Dev</i>
Longitudinal ( $0^\circ$ )	25.51, 0.73	25.72, 0.91	987.80, 19.98
Diagonal ( $45^\circ$ )	15.68, 0.27	16.22, 0.27	741.78, 20.28
Transverse ( $90^\circ$ )	14.35, 0.08	14.56, 0.05	738.77, 7.91
Default ( $+45^\circ/-45^\circ$ )	18.90, 0.53	19.36, 0.39	768.01, 33.31

Table 2. Tension test results

A one-way analysis of the variance (ANOVA) was completed in order to consider the equivalence of the population means for the four raster orientations. The results, appearing in Table 3, include a calculated F-test statistic of  $F(3,16) = 490.98$  and a  $p$ -value of 0.0001, indicating a significant difference between some or all of the mean ultimate strength (UTS) values associated with the four raster orientations at a level of significance of  $\alpha = 0.05$ . The coefficient of determination associated with this analysis was  $R^2 = 0.9886$ .

Source	DF	SS	MS	F	P
Raster Angle	3	363.991	121.330	460.98	0.0001
Error	16	4.211	0.263		
Total	19	368.202			

Table 3. ANOVA results comparing mean ultimate tensile strengths of 4 raster orientations

Further analysis in the form of post hoc comparisons was performed to determine which raster orientations differed in mean UTS. Tukey's method (Montgomery, 2009), creating a set of 95% simultaneous confidence intervals for the difference between each pair of means, indicated that the difference was significant for all pairwise comparisons of mean UTS values (Table 4). The difference between the mean UTS of the longitudinal rasters (25.72) and that of the transverse rasters (14.56) was the most significant. These results confirm that raster orientation has a significant effect on the tensile strengths of the FDM specimens. Tensile strength is thus verified to be affected by the directional processing and subsequent directionality of the polymer molecules, signifying an anisotropic property.

Raster Orientation (i)	Raster Orientation (j)	Difference of Mean UTS (i-j)	95% Confidence Interval	
			Lower Bound	Upper Bound
Longitudinal	45-Degree	9.50*	8.579	10.437
	Transverse	11.16*	10.235	12.093
	Default	6.36*	5.438	7.296
45-Degree	Transverse	1.66*	0.727	2.585
	Default	-3.14*	-4.07	-2.212
Transverse	Default	-4.8*	-5.726	-3.868

\* Mean difference is significant at the 0.05 level

Table 4. Post hoc Tukey HSD multiple comparisons of mean tensile strengths

The quantitative data analysis was followed by detailed physical inspection of the specimens at both macro and microscopic levels. Macroscopically, the fracture patterns of the specimens varied somewhat as a function of the raster orientation of the two-dimensional layers and the resulting weakest path for crack propagation (Figure 5). The 90° specimens failed in the transverse direction and the 45° specimens failed along the 45° line. The 0° specimens failed primarily in the transverse direction, although there was some fiber pullout and delamination intermittently evident as well. The +45°/-45° specimens broke at intersecting fracture paths along ±45°, resulting in a saw-tooth fracture pattern across the specimen width. It is likely that fracture paths controlled by weak interlayer bonding are affected by the residual stresses that result from the volumetric shrinkage of the polymer layers during solidification and cooling. In addition, interlayer porosity and air gaps serve to reduce the actual load-bearing area across the layers, providing an easy fracture path.

In specimens with the longitudinal (0°) raster orientation, the molecules tend to align along the stress axis direction. This produces the strongest individual two-dimensional layers subjected to tension loading. During the testing of these specimens, stress whitening due to

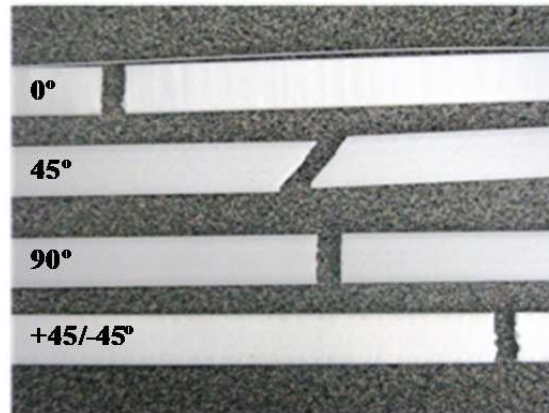


Fig. 5. Failure modes of the specimens with each of the four raster orientations

craze formation and growth was observed to develop prior to reaching the yield stress. Failure occurred at whitened areas from plastic deformation where some evidence of localized fiber delamination was observed. The fracture surfaces were further analyzed with a scanning electron microscope, and displayed failure that was predominantly brittle in nature with localized micro-shearing on each fiber face (Figure 6). The tensile strength of these specimens is thus more heavily dependent on the strength of the ABS monofilament than specimens with fibers running at orientations other than  $0^\circ$  with the stress axis (Rodriguez et al., 2001).

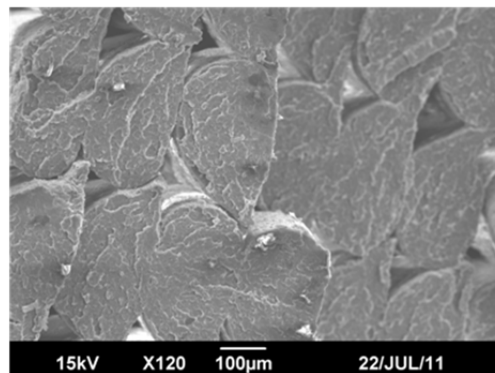


Fig. 6. SEM image of fracture surface of a  $0^\circ$  raster specimen

In contrast, the specimens with transverse ( $90^\circ$ ) raster orientations did not display obvious crazing during testing, and failure occurred predominantly at the weak interface between layered ABS fibers (Figure 7). These specimens experienced brittle interface fracture. Weak interlayer bonding or some amount of interlayer porosity was evident in the failure of many of the specimens with raster orientations other than  $0^\circ$ , and appeared to be the cause of layer delamination along the fiber orientation during loading. The tensile strength of these specimens depended much more heavily upon the fiber-to-fiber fusion and any air gap resulting between the fibers, as opposed to the strength of the fibers themselves.



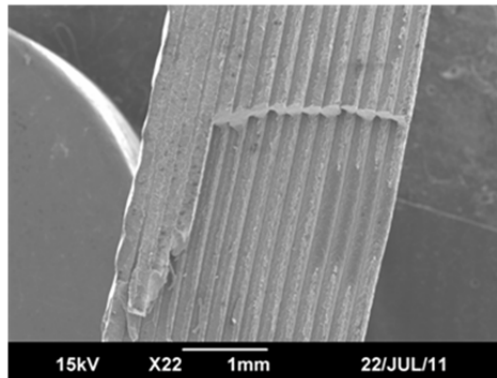


Fig. 7. SEM image of fracture surface of a 90° raster specimen

Under microscopic examination, the +45°/-45° specimens displayed multiple failures of individual raster fibers in both shear and tension (figure 8a). Failure occurred by the pulling and eventual rupturing of individual fibers whereby the material separated at a +45°/-45° angle relative to the tensile load, creating the saw-tooth like appearance evident at the macro-scale (figure 5). Failure of the 45° raster specimens was similar to that of the default +45°/-45° in that it was a brittle shear failure on each of the individual fibers at the microscopic level, as each raster was pulled in tension and failed at 45 degrees relative to the loading axis (figure 8b). Macroscopically, the samples also displayed a characteristic shear failure along the 45° line with the tensile load (figure 5).

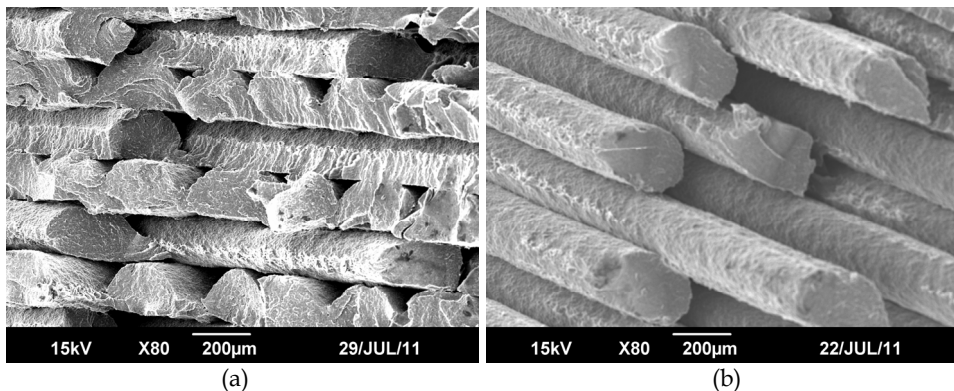


Fig. 8. SEM image of fracture surfaces of (a) +45°/-45° and (b) 45° raster specimen

The air gap that forms during fabrication and remains present between fibers of the FDM specimens is a significant factor in considering tensile ultimate and yield strengths and comparing these properties to those of injection molded ABS specimens. Although the FDM machine setting indicated a desired air gap of 0.0 mm, the fiber geometry inherently causes the presence of triangular air voids as seen in the SEM image in Figure 9. These voids influence the effective tensile strengths and effective elastic moduli of the FDM parts by decreasing the physical cross-sectional area of material specimens. This is in part why the

injection molded specimens displayed tensile strengths greater than that of any of the FDM parts, achieving a mean yield and ultimate tensile strength of 26.95 and 27.12 MPa respectively. The mean UTS achieved by the 0° raster specimens was closest to that of the injection molded specimens, representing 94.8% of its value.

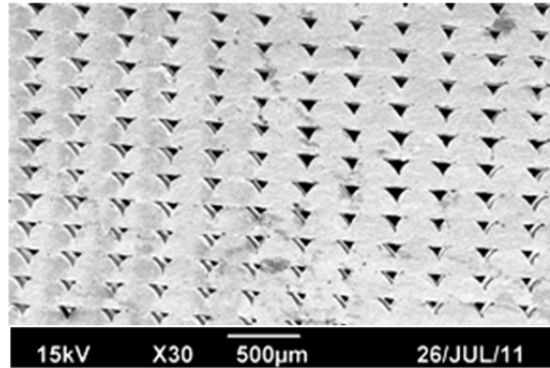


Fig. 9. SEM image of air voids seen on fractured 0° raster specimen

### 3.2 Compression testing

A summary of the compression test results, as displayed in Table 5, shows strengths that are higher than those obtained in tension testing. Higher compressive strengths are often observed in polymers, and specifically for bulk ABS materials (Ahn et al., 2002). In this study, the average tensile yield strength for FDM specimens was 56% of the average compressive yield strength for FDM specimens. The mean compressive ultimate and yield strengths (0.2% offset) were found to be the largest for the 90° raster orientation, 34.69 and 29.48 MPa respectively. The 45° raster specimens displayed the smallest mean yield strength, 24.46 MPa, representing 82.97% of the yield strength of the 90° raster specimens. The mean yield strength for the injection molded specimens was 35.50 MPa, a value higher than any of the FDM specimens tested. The 90° raster specimens performed the most closely to the injection molded parts, achieving a mean yield strength that was 83.0% of that of the molded specimens.

<i>Raster Orientation</i>	<i>Mean Yield Strength (MPa), Std Dev</i>	<i>Mean Ultimate Strength (MPa), Std Dev</i>	<i>Mean Effective Modulus</i>
Longitudinal (0°)	28.83, 1.16	32.32, 0.58	402.64, 3.64
Diagonal (45°)	24.46, 0.30	33.43, 0.20	417.20 10.06
Transverse (90°)	29.48, 0.75	34.69, 0.99	382.21, 10.31
Default (+45°/-45°)	28.14, 0.64	34.57, 0.86	410.44, 11.23

Table 5. Compression test results

Although mean ultimate strengths are provided in Table 5, it is typically difficult to pinpoint the instance of rupture in compression loading. Most plastics do not exhibit rapid fracture in compression and the focus is therefore on measuring the compressive yield stress at the point of permanent yield on the stress-strain curve (Riley et al., 2006). Although many of the FDM specimens failed by separation between layers, resulting in two or three distinct

pieces, yield stresses were analyzed for consistency and to allow for comparisons with that of the injection molded specimens. As a result, a one-way ANOVA was conducted to compare the effect of raster orientation on mean compressive yield strengths in 0°, 45°, 90°, and +45°/-45° conditions. The test indicated that raster orientation had a significant effect on mean compressive yield strength at the  $p < 0.05$  level for the four conditions,  $F(3, 16) = 31.25$ ,  $p = 0.0001$ . Post hoc comparisons using the Tukey HSD test indicated that this significance was limited to and specifically in regard to comparisons with the 45° diagonal condition. The mean yield strength for the 45° raster orientation (24.46 MPa) was significantly different (lower) than that of the other three raster orientations (Table 6), while all other paired comparisons indicated statistically insignificant differences in the mean yield strengths.

Inspection of the failed compression specimens provided additional evidence that the 45° raster specimens were significantly weaker in compression than the other raster orientations. The specimens ultimately separated into two or three pieces, following the displacement of the cylinder's top relative to its bottom, as seen in Figure 10. This distortion occurred as a result of the shearing or sliding along the 45° rasters as the specimens was subjected to an axial compressive load. The other three raster orientations displayed less distortion prior to failure and had mean compressive yield strengths that were significantly larger than that of the 45° raster specimens.

Raster Orientation ( <i>i</i> )	Raster Orientation ( <i>j</i> )	Difference of Mean Yield Strength ( <i>i-j</i> )	95% Confidence Interval	
			Lower Bound	Upper Bound
Longitudinal	45-Degree	4.365*	2.739	5.991
	Transverse	-0.653	-2.279	0.973
	Default	0.683	-0.943	2.309
45-Degree	Transverse	-5.018*	-6.644	-3.392
	Default	-3.682*	-5.308	-2.056
Transverse	Default	1.336	-0.290	2.962

\* Mean difference is significant at the 0.05 level

Table 6. Post hoc Tukey HSD multiple comparisons of mean yield compressive strengths

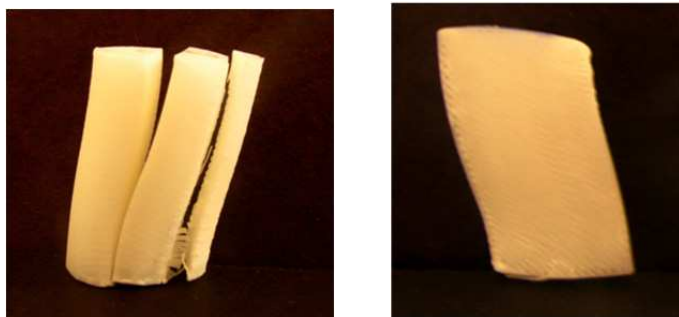


Fig. 10. Photos of failed 45° raster specimens under compression loading

### 3.3 Flexural testing

Three-point bend tests were completed in order to study the flexural properties of the FDM specimens. Following preliminary testing, a three-inch gage length or span between the outermost points was used for all tests (Figure 11). Flexural strengths were found to be greater than tensile strengths for each raster orientation because the specimens are subjected to both tensile and compressive stresses during bending (Riley et al., 2006). In addition, the three-point test configuration results in the measurement of the maximum strength at the outermost fiber of the beam specimens.

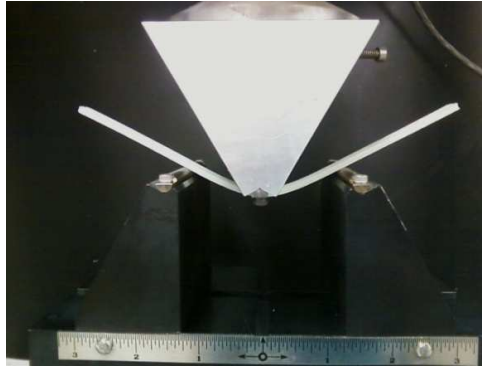


Fig. 11. Three-point bend test configuration

The results of the three-point bend flexural tests are displayed in Table 7. The mean ultimate strength value is the highest for the  $0^\circ$  fiber orientation (38.1 MPa), as was the case during tensile testing. The  $+45^\circ/-45^\circ$  orientation had the next highest flexural strength values, followed by  $45^\circ$  and then  $90^\circ$  ( $23.3$  MPa) orientations. Consequently, the flexural test results in Table 7 display the same trend as the tensile test results in Table 2. The flexural strength of the  $90^\circ$  raster specimen was only 60.9% of that of the  $0^\circ$  specimen.

<i>Raster Orientation</i>	<i>Mean Yield Strength (MPa), Std Dev</i>	<i>Mean Ultimate Strength (MPa) Std Dev</i>	<i>Mean Effective Modulus (MPa), Std Dev</i>
Longitudinal ( $0^\circ$ )	34.2, 2.6	38.1, 2.3	1549.0, 327.3
Diagonal ( $45^\circ$ )	21.3, 0.2	25.7, 0.6	1250.0, 36.1
Transverse ( $90^\circ$ )	20.8, 0.9	23.3, 1.6	1269.7, 149.6
Default ( $+45^\circ/-45^\circ$ )	26.5, 0.7	32.2, 0.5	1438.6, 34.7

Table 7. Flexural test results

Similar to compression testing, however, not all of the specimens ruptured at failure. The  $0^\circ$  raster specimens and the  $+45^\circ/-45^\circ$  specimens never fractured, warranting further analysis to be based upon yield rather than ultimate strengths for consistency. A one-way ANOVA was completed and determined that raster orientation had a significant effect on mean flexural yield strengths at the  $p < 0.05$  level for the four conditions, with  $F(3, 16) = 96.44$  and  $p = 0.0001$  (Table 8). The coefficient of determination associated with this analysis was  $R^2 = 0.9476$ .

Source	DF	SS	MS	F	P
Raster Angle	3	582.55	194.18	96.44	0.0001
Error	16	32.22	2.01		
Total	19	614.77			

Table 8. One-way ANOVA results for flexural testing

Post hoc analysis further indicated a significant difference between all paired mean comparisons other than that of the 45° raster condition (21.3 MPa) in comparison to the 90° raster condition (20.8 MPa). These flexural strength results further confirm that the raster orientation of the FDM specimens contributes to directionally dependent performance. The specimen fracture patterns for the 45° and the 90° specimens were similar to those described for the tensile testing. In contrast, the 0° and the +45°/-45° specimens never fractured during three-point bend testing, but retained some degree of permanent deformation.

Examination of the fracture surfaces of those specimens that broke into two pieces, i.e. the 45° raster specimens and the 90° specimens, revealed that failure initiated on the side of the part that was under tension loading. As fracture began, the specimen initially remained together by unbroken fibers on portion of it that was in compression. Crack propagation along load direction was erratic and not uniform. This is apparent in Figure 12, which displays clusters of fibers that have bent and then ruptured individually in a catastrophically brittle manner.

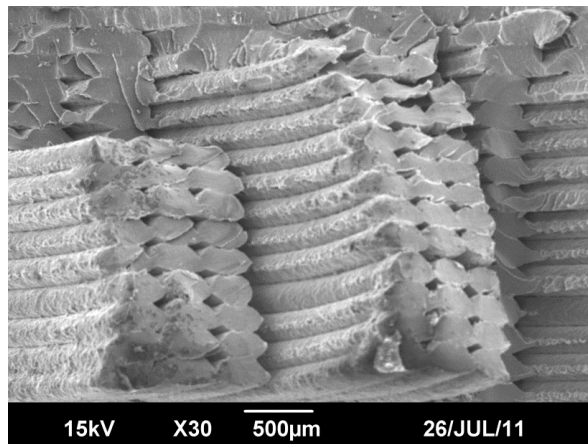


Fig. 12. SEM image of the fracture surface of a 45° raster specimen after flexural loading

Specimens with 0° raster orientation will have fibers that are able to offer more resistance to bending because they are parallel to the bending plane. There is more fiber length over which the load can be distributed. As the raster angle increases to 45° or 90°, the fiber inclination relative to the plane of bending produces rasters with smaller lengths. This results in a net decrease in the ability of the specimen to resist the load. This effect is observed in Figure 13 where the 90° raster specimen shows little evidence of bending. The bottom of the specimen shows a large flat area initially affected by the failure of several

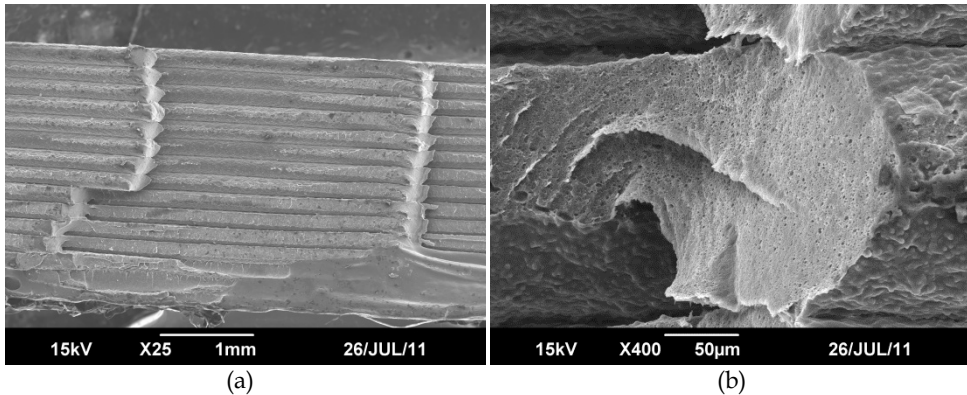


Fig. 13. SEM image of fractured 90° flexural specimen magnified (a) 25X and (b) 400X

rasters, from which the crack then splits to the right and left and eventually climbs, as seen in the shear failure of individual rasters in layers. Upon closer microscopic examination, it was observed that individual rasters showed shear failure with a clearly defined exaggerated shear lip on the top of each fiber; something that was not observed in the analysis of 90° raster specimens that failed in tension testing (Figure 7). In both the 45° and the 90° raster specimens, there is little localized plastic deformation before failure initiates and fibers begin to break.

### 3.4 Impact testing

The impact study utilized an Izod test configuration with a notched specimen held as a vertical cantilevered beam as shown in Figure 14. In this position, the material was subjected to a load in the form of an impact blow from a weighted pendulum hammer striking the notched side of the specimen. The test measures the impact energy or notch toughness, and the results are expressed in energy absorbed per unit of thickness at the notch in units of J/cm. The impact energy absorbed by the specimen during failure is measured by calculating the change in the potential energy of the hammer. The change in potential energy is proportional to difference in the height of the hammer from its initial position to the maximum height achieved after impact.

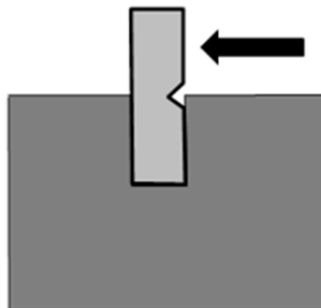


Fig. 14. Izod impact test configuration

Impact tests were completed on 10 specimens with each of the four raster orientations. The mean impact energy results are displayed in Table 9. The absorbed energy was the highest for the longitudinal ( $0^\circ$ ) fiber orientation (2.989 J/cm) and the lowest for the transverse ( $90^\circ$ ) orientations (1.599 J/cm). The  $45^\circ$  and  $+45^\circ/-45^\circ$  default specimens broke with mean impact resistances between those of the  $0^\circ$  and  $90^\circ$  specimens.

Raster Orientation	Mean Impact Energy (J/cm)	Standard Deviation	Fracture Type
Longitudinal ( $0^\circ$ )	2.991	0.103	Hinged
Diagonal ( $45^\circ$ )	2.339	0.483	Hinged & Complete
Transverse ( $90^\circ$ )	1.599	0.014	Complete
Default ( $+45^\circ/-45^\circ$ )	2.514	0.338	Hinged & Complete

Table 9. Impact test results

The relative impact strengths of the four raster orientations correlated well with the tensile strength results. In addition, the variation of the impact strengths was smallest for the transverse orientation (Figure 15), coinciding with the variation of the tensile test results.

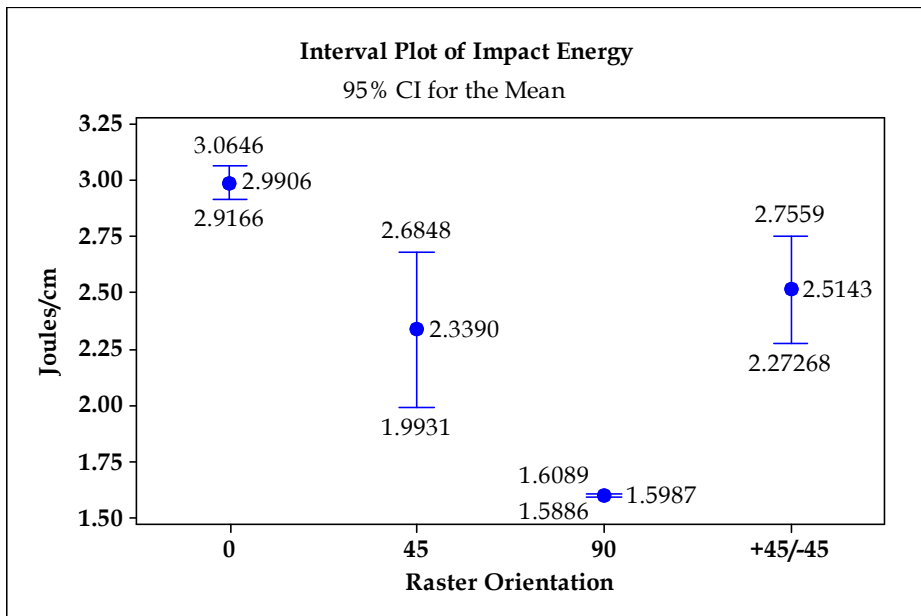


Fig. 15. Interval plot of impact test results

A one-way ANOVA was conducted to compare the effect of raster orientation on mean impact energies in  $0^\circ$ ,  $45^\circ$ ,  $90^\circ$ , and  $+45^\circ/-45^\circ$  conditions. There was a significant effect of raster orientation on impact energies at the  $p < 0.05$  level for the four conditions, with  $F(3, 36) = 37.23$ ,  $p = 0.0001$ . Post hoc comparisons using indicated that the mean impact energy for the  $45^\circ$  diagonal condition (2.339 J/cm) did not significantly differ from that of the  $+45^\circ/-45^\circ$  condition (2.514 J/cm), applying a 95% confidence interval (Table 10). All other paired

comparisons indicated statistically significant differences in mean impact energies. These results suggest that impact strength has anisotropic characteristics.

Raster Orientation ( <i>i</i> )	Raster Orientation ( <i>j</i> )	Difference of Mean Impact Energy ( <i>i-j</i> )	95% Confidence Interval	
			Lower Bound	Upper Bound
Longitudinal	45-Degree	0.652*	0.291	1.012
	Transverse	1.392*	1.031	1.753
	Default	0.473*	0.116	0.837
45-Degree	Transverse	0.740*	0.379	1.101
	Default	-0.175	-0.536	0.184
Transverse	Default	-0.916*	-1.276	-0.555

\* Mean difference is significant at the 0.05 level

Table 10. Post hoc Tukey HSD multiple comparisons of mean impact energies

Inspection indicated that the fracture patterns of the specimens varied as a function of the raster orientations. The longitudinal ( $0^\circ$ ) and transverse ( $90^\circ$ ) pieces fractured along a path oriented  $90^\circ$  to the length of the specimen. The fracture surface appeared smooth along the layers of each of the transverse specimens, all of which experienced clean and complete separation of the specimen into two discrete pieces. Weak interfaces parallel to the crack front affected the transverse raster specimens by providing a straightforward path for crack propagation, resulting in the least amount of energy absorption. Failure initiated from the side on the notch where the energy absorption was greatest, thus causing the rasters to fracture longitudinally along the length of the fiber through several layers until the energy adsorption decreased significantly and the sample broken in half (Figure 16a). Upon closer examination, it can be seen that individual fibers plastically deformed and twisted at the ends upon catastrophic failure, whereby halves of the samples separated (Figure 16b).

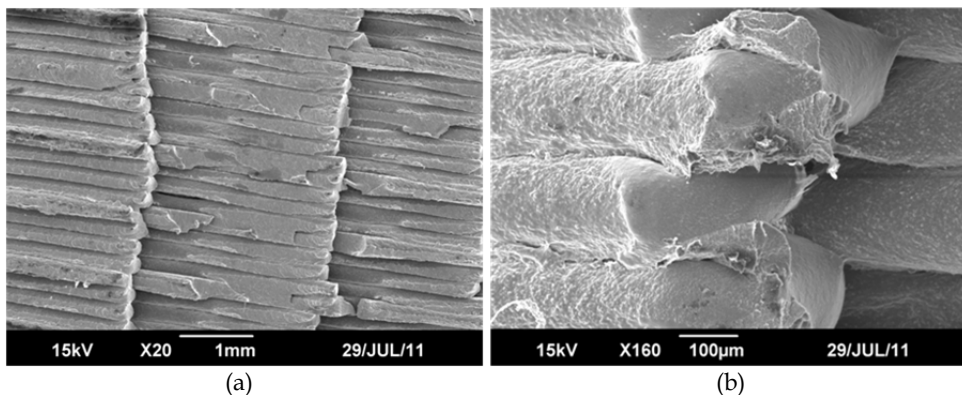


Fig. 16. SEM image of fractured  $90^\circ$  impact specimen magnified (a) 20X and (b) 160X

The fracture surfaces of the  $0^\circ$  raster specimens were macroscopically rougher, in contrast, displaying slightly jagged edges of individual broken fibers along the transverse fracture



plane. Interlayer delamination was also evident and resulted in hinged specimens at failure. Figure 17 displays a  $0^\circ$  specimen where the slightly varied fiber length is evident, along with the formation of a hinge. The longitudinal specimens had the highest mean impact strength, correlating well with the results of three-point bend tests.

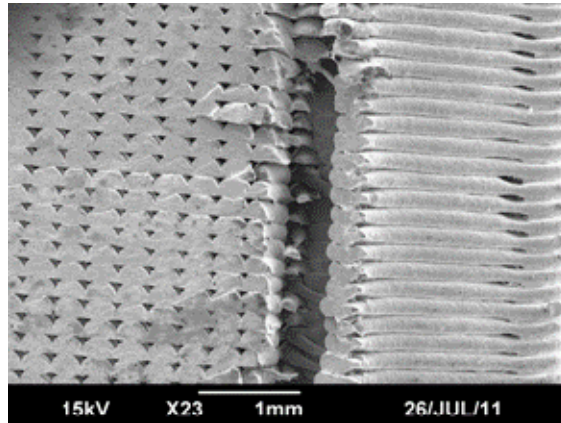


Fig. 17. SEM image of impact fractured  $0^\circ$  raster specimen

Weak interfaces running at  $\pm 45^\circ$  to the crack front require relatively high amounts of energy as a result of a mixed fracture mode. As a result, a rougher texture was evident for the fracture surfaces of the default raster specimens, and several hinged as shown on the bottom of Figure 18a. The fracture pattern of the  $45^\circ$  specimens, in contrast, fractured more consistently along the  $45^\circ$  maximum shear plane as shown on the top of Figure 18a. The macroscopic roughness of the fracture surface was the result of the varying fiber lengths, evident in the SEM image of Figure 18b.

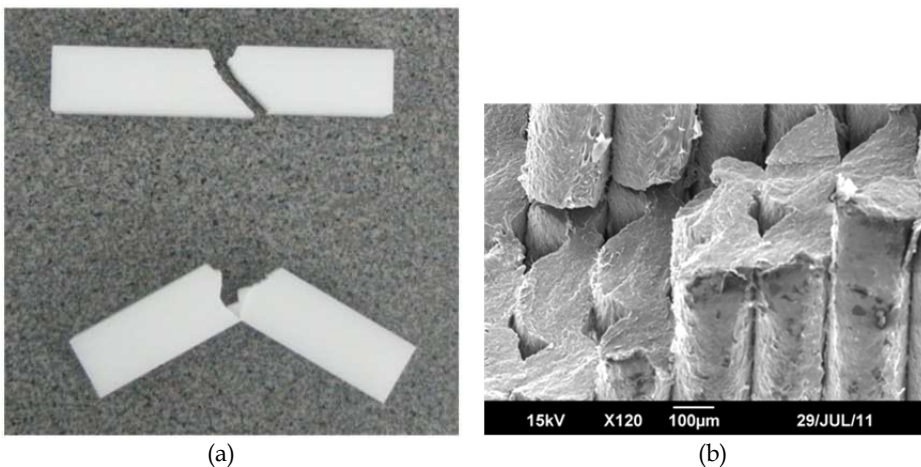


Fig. 18. (a) Fracture patterns of  $45^\circ$  &  $+45^\circ/-45^\circ$  specimens; (b) SEM image of impact fractured  $45^\circ$  raster specimen

### 3.5 Tension-tension fatigue testing

In analyzing the feasibility of fused deposition modeling to fully evolve into a rapid manufacturing tool, it is important to assess the fatigue properties of FDM specimens and their dependence upon raster orientation. A comprehensive fatigue study is warranted and is currently underway by the authors. At this time, however, a pilot fatigue study utilizing a tension-tension loading configuration has been completed. The fatigue tests utilized specimens originally with natural undamaged surfaces. The maximum load of the fatigue cycles was set to 70% of the mean failure load as determined in the static tensile tests for each specific raster orientation. The minimum cycle load was set as 1/10 of the maximum load, and the resulting stress ratio  $R$  for the fatigue tests was 0.1. The value of 70% of the mean failure load was selected following a preliminary study focused on determining a reasonable compromise between the occurrences of excessively long fatigue lives and being too close to the static strength.

All fatigue tests were performed at room temperature. To eliminate any heating effects due to considerable strains, the fatigue loading was applied at a low frequency, 0.25 Hz. The specimen surface was observed during testing and the number of cycles to final failure was determined. The test results appear in Table 11. The 45° raster orientation fractured with the smallest mean number of cycles to failure (1312), representing only 26.7% of that of the +45°/-45° raster orientation (4916).

Raster Orientation	Mean No. Cycles to Failure	Standard Deviation
Longitudinal (0°)	4557	694
Diagonal (45°)	1312	211
Transverse (90°)	1616	195
Default (+45°/-45°)	4916	150

Table 11. Tension-tension fatigue test results

A one-way ANOVA was completed in order to consider the equivalence of the mean number of cycles to failure for the four raster orientations. The results, appearing in Table 12, provide a calculated F-test statistic of  $F(3,16) = 124.95$  and a  $p$ -value of 0.0001, indicating a significant difference between some or all of the mean cycle values associated with the four raster orientations at a level of significance of  $\alpha = 0.05$ . The resulting coefficient of determination associated with this analysis was  $R^2 = 0.9591$ .

Source	DF	SS	MS	F	P
Raster Angle	3	54093034	18031011	124.95	0.0001
Error	16	2308959	144310		
Total	19	56401993			

Table 12. One-way ANOVA results for tension-tension fatigue testing

Tukey post hoc comparisons indicated that the difference between the mean number of cycles to failure was not significant for the pairwise comparisons of 0° with +45°/-45°, or 45° with 90° raster specimens. All other pairwise comparisons were significantly different.

These results confirm that certain raster orientations have a significant effect on the tension-fatigue properties of the FDM specimens.

The failure modes of the specimens were similar to those for static tension testing (Figure 5), except that several of the  $0^\circ$  raster specimens fractured with a more uneven and almost toothed appearance during fatigue testing. This is shown in Figure 19a where the clusters of rasters have broken at various fiber lengths showing an erratic crack path most probably driven by the areas of weakest fiber bonds and voids between fibers. This SEM image also shows the smooth, brittle, tensile failure on each individual raster face.

The fracture surfaces of the  $+45^\circ/-45^\circ$  raster specimens, in contrast, showed a mixed mode repeated failure of individual fibers by shearing and tension (Figure 19b). Upon close examination of the individual raster faces, failure initiation sites can be observed at multiple locations. In areas of closely bonded clusters of fibers, "river patterns" can be observed and are believed to occur at large crack growth rates. At the same time, patterns resembling "fish scales" are observed and are often an indication of small crack growth rates. This change of the pattern indicates the existence of a dynamic transition of failure mode.

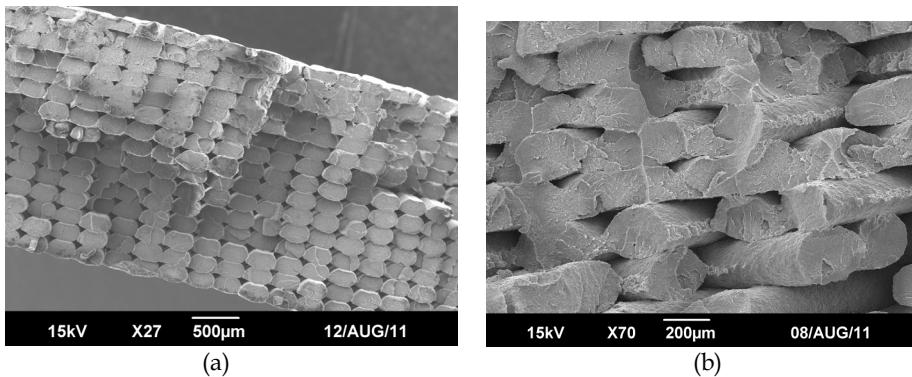


Fig. 19. SEM images of fatigue fractured specimens with: (a)  $0^\circ$  rasters (b)  $+45^\circ/-45^\circ$  rasters

There was some level of correlation between the tension-tension fatigue results and the static tension test results. While the  $0^\circ$  raster orientation achieved the maximum tensile strength, the  $+45^\circ/-45^\circ$  specimens survived the most fatigue cycles to failure on average. However, the mean number of cycles to failure for the  $0^\circ$  raster orientation was not found to be statistically different than the  $+45^\circ/-45^\circ$  specimens at a level of significance of  $\alpha = 0.05$ .

Although these fatigue tests only serve the purpose of a pilot study, the results indicate that the directionality of the polymer molecules and the presence of air gaps and porosity result in anisotropic behaviour of FDM specimens under tension-fatigue loading.

#### 4. Conclusion

The mechanical properties of ABS specimens fabricated by fused deposition modelling display anisotropic behaviour and are significantly influenced by the orientation of the layered rasters and the resulting directionality of the polymer molecules. The presence of air

gaps and the quantity of air voids between the rasters or fibers additionally influences the strength and effective moduli in regard to all of the tests completed in this study.

- a. Tension tests indicate that the ultimate and yield strengths are the largest for the  $0^\circ$  raster orientation, followed by the  $+45^\circ/-45^\circ$ ,  $45^\circ$ , and  $90^\circ$  orientations in descending order. The differences between mean ultimate tensile strengths are significant for all pairwise comparisons of different raster orientations. Fracture paths are affected by the directionality of the polymer molecules and the strength of individual layers. The longitudinal specimens benefit from the alignment of molecules along the stress axis.
- b. The compression test data indicates that the  $45^\circ$  raster specimens are significantly weaker in compression than the other raster orientations, and they distort prior to failure as a result of shearing along the raster axes. The other three raster orientations have mean yield strengths that are significantly larger than that of the  $45^\circ$  raster specimens, and that are statistically equal to each other at a level of significance of  $\alpha = 0.05$ .
- c. The results of both three-point bend and impact tests correlate well with tension test results, again indicating that the yield strengths are the largest for the  $0^\circ$  raster orientation, followed by the  $+45^\circ/-45^\circ$ ,  $45^\circ$ , and  $90^\circ$  orientations in descending order. The  $0^\circ$  rasters offer the most resistance to bending due to the largest effective raster lengths. As raster angle increases, the effective length and associated flexural and impact strengths decrease. Mean flexural and impact strengths are significantly affected by raster orientations, with the pairwise comparison of  $45^\circ$  and  $90^\circ$  rasters as the only one with no statistical difference.
- d. Preliminary tension-tension fatigue tests indicate anisotropic behaviour on the basis of raster orientations. The difference between the mean number of cycles to failure was statistically significant for all pairwise comparisons other than  $0^\circ$  with  $+45^\circ/-45^\circ$ , and  $45^\circ$  with  $90^\circ$  raster specimens. Failure modes are similar to those seen in static tension tests.

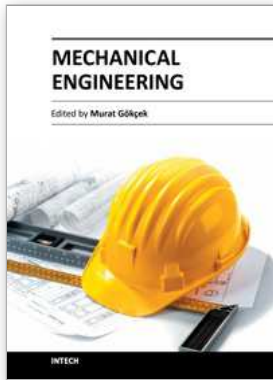
The results of this project are useful in defining the most appropriate raster orientation for FDM components on the basis of their expected in-service loading. Results are also useful to benchmark future analytical or computational models of FDM strength or stiffness as a function of void density. Additional research currently in progress includes a thorough fatigue analysis of FDM specimens with varying raster orientations.

## 5. References

- Ahn, S., Montero, M., Odell, D., Roundy, S. & Wright, P. (2002), Anisotropic Material Properties of Fused Deposition Modeling ABS. *Rapid Prototyping Journal*, Vol. 8, No. 4, pp. 248 –257, ISSN 1355-2546
- ASTM Standard D256. (2010). Standard Test Methods for Determining the Izod Pendulum Impact Resistance of Plastics. *ASTM International*, West Conshohocken, Pennsylvania, DOI: 10.1520/D0256-10, Available from: <www.astm.org>
- ASTM Standard D695. (1996). Standard Test Method for Compressive Properties of Rigid Plastics. *ASTM International*, West Conshohocken, Pennsylvania, DOI: 10.1520/D0695-10, Available from: <www.astm.org>
- ASTM Standard D790. (2010). Standard Test Methods for Flexural Properties of Unreinforced and Reinforced Plastics and Electrical Insulating Materials. *ASTM*

- International*, West Conshohocken, Pennsylvania, DOI: 10.1520/D0790-10, Available from: <www.astm.org>
- ASTM Standard D3039/D3039M – 08. (2008). Standard Test Method for Tensile Properties of Polymer Matrix Composite Materials. *ASTM International*, West Conshohocken, Pennsylvania, DOI: 10.1520/D3039\_D3039M-08, Available from: <www.astm.org>
- ASTM Standard D3479. (2007). Standard Test Method for Tension-Tension Fatigue of Polymer Matrix Composite Materials. *ASTM International*, West Conshohocken, Pennsylvania, DOI: 10.1520/D3479M-96R07, Available from: <www.astm.org>
- Caulfield, B., McHugh, P. & Lohfeld, S. (2007). Dependence of mechanical properties of polyamide components on build parameters in the SLS process. *Journal of Materials Processing Technology*, Vol. 182, pp. 477–488, ISSN 0924-0136
- Chua, C., Feng, C., Lee, C. & Ang G. (2005). Rapid investment casting: direct and indirect approaches via model maker II. *International Journal of Advanced Manufacturing Technology*, Vol. 25, pp. 11–25, ISSN
- Es Said, O., Foyos, J., Noorani, R., Mendelson, M., Marloth, R. & Pregger, B. (2000). Effect of layer orientation on mechanical properties of rapid prototyped samples. *Materials and Manufacturing Processes*, Vol. 15, No. 1, pp. 107–22, ISSN 1532-2475.
- Lee, B., Abdullah, J. & Khan, Z. (2005). Optimization of rapid prototyping parameters for production of flexible ABS object. *Journal of Materials Processing Technology*, Vol. 169, pp.54–61, ISSN 0924-0136
- Lee, C., Kim, S., Kim, H. & Ahn, S. (2007). Measurement of anisotropic compressive strength of rapid prototyping parts. *Journal of Materials Processing Technology*, Vol. 187–188, pp. 627–630, ISSN 0924-0136
- Montgomery, D. (2009). *Design and Analysis of Experiments* (7th Edition), John Wiley & Sons, ISBN 978-0-470-12866-4, Hoboken, New Jersey
- Odian, G. (2004). *Principles of Polymerization*(4th Edition), John Wiley & Sons, ISBN 978-0-471-27400-1, Hoboken, New Jersey
- Riley, W., Sturges, L. & Morris, D. (2006). *Mechanics of Materials* (6th Edition), John Wiley & Sons, ISBN 978-0-471-70511-6, Hoboken, New Jersey
- Rodriguez, J., Thomas, J. & Renaud, J. (2001). Mechanical Behavior of Acrylonitrile Butadiene Styrene (ABS) Fused Deposition Materials. Experimental Investigation. *Rapid Prototyping Journal*, Vol. 7, No. 3, pp. 148-158, ISSN 1355-2546
- Rodriguez, J., Thomas, J. & Renaud, J. (2003). Mechanical behavior of acrylonitrile butadiene styrene fused deposition materials modeling. *Rapid Prototyping Journal*, Vol. 9, No. 4, pp. 219-230, ISSN1355-2546
- Sood A., Ohdar R. & Mahapatra, S. (2010). Parametric appraisal of mechanical property of fused deposition modelling processed parts. *Materials & Design*, Vol. 31, No. 1, pp. 287–95, ISSN 0261-3069
- Sood, A., Ohdar, R. & Mahapatra, S. (2011). Experimental investigation and empirical modeling of FDM process for compressive strength improvement. *Journal of Advanced Research*, DOI:10.1016/j.jare.2011.05.001, ISSN 2090-1232
- Sun, Q., Rizvi, G., Bellehumeur, C. & Gu, P. (2008). Effect of processing conditions on the bonding quality of FDM polymer filaments. *Rapid Prototyping Journal*, Vol. 14, No. 2, pp. 72 – 80, ISSN 1355-2546

Upcraft, S. & Fletcher, R. (2003). The rapid prototyping technologies. *Assembly Automation*, Vol.23, No.4, pp. 318-330, ISSN 0144-5154



## **Mechanical Engineering**

Edited by Dr. Murat Gokcek

ISBN 978-953-51-0505-3

Hard cover, 670 pages

**Publisher** InTech

**Published online** 11, April, 2012

**Published in print edition** April, 2012

The book substantially offers the latest progresses about the important topics of the "Mechanical Engineering" to readers. It includes twenty-eight excellent studies prepared using state-of-art methodologies by professional researchers from different countries. The sections in the book comprise of the following titles: power transmission system, manufacturing processes and system analysis, thermo-fluid systems, simulations and computer applications, and new approaches in mechanical engineering education and organization systems.

### **How to reference**

In order to correctly reference this scholarly work, feel free to copy and paste the following:

Constance Ziemian, Mala Sharma and Sophia Ziemian (2012). Anisotropic Mechanical Properties of ABS Parts Fabricated by Fused Deposition Modelling, Mechanical Engineering, Dr. Murat Gokcek (Ed.), ISBN: 978-953-51-0505-3, InTech, Available from: [http://www.intechopen.com/books/mechanical-engineering/anisotropic-mechanical-properties-of-abs-parts-fabricated-by-fused-deposition-modeling-](http://www.intechopen.com/books/mechanical-engineering/anisotropic-mechanical-properties-of-abs-parts-fabricated-by-fused-deposition-modeling)

# **INTECH**

open science | open minds

### **InTech Europe**

University Campus STeP Ri  
Slavka Krautzeka 83/A  
51000 Rijeka, Croatia  
Phone: +385 (51) 770 447  
Fax: +385 (51) 686 166  
[www.intechopen.com](http://www.intechopen.com)

### **InTech China**

Unit 405, Office Block, Hotel Equatorial Shanghai  
No.65, Yan An Road (West), Shanghai, 200040, China  
中国上海市延安西路65号上海国际贵都大饭店办公楼405单元  
Phone: +86-21-62489820  
Fax: +86-21-62489821

© 2012 The Author(s). Licensee IntechOpen. This is an open access article distributed under the terms of the [Creative Commons Attribution 3.0 License](#), which permits unrestricted use, distribution, and reproduction in any medium, provided the original work is properly cited.